Anisotropic electronic band structure of intrinsic Si(110) studied by angle-resolved photoemission spectroscopy and first-principles calculations

Stephane Yu Matsushita,[1] Akari Takayama,[2,*] Erina Kawamoto,[1] Chunping Hu,[3,†] Satoshi Hagiwara,[3] Kazuyuki Watanabe,[3] Takashi Takahashi,[1,2] and Shozo Suto[1,‡]

[1]*Department of Physics, Graduate School of Science, Tohoku University, Sendai 980-8578,Japan*

[2]*WPI Research Center, Advanced Institute for Materials, Tohoku University, Sendai 980-8577, Japan*

[3]*Department of Physics, Tokyo University of Science, Shinjyuku-ku, Tokyo 162-8601, Japan*

(Received 21 December 2016; revised manuscript received 27 August 2017; published 14 September 2017)

We have studied the electronic band structure of the hydrogen-terminated Si(110)-(1×1) [H:Si(110)-(1×1)] surface using angle-resolved photoemission spectroscopy (ARPES) and first-principles calculations in the framework of density functional theory with local density approximation (LDA). The bulk-truncated H:Si(110)-(1×1) surface is a good template to investigate the electronic band structure of the intrinsic Si(110). In the ARPES spectra, seven bulk states and one surface state due to the H-H interaction are observed clearly. The four bulk states consisting of Si $3p_{xy}$ orbitals exhibit anisotropic band dispersions along the high symmetric direction of $\overline{\Gamma}$-$\overline{X}$ and $\overline{\Gamma}$-$\overline{X}'$ directions, where one state shows one-dimensional character. The calculated band structures show a good agreement with the experimental results except the surface state. We discuss the exact nature of electronic band structures and the applicability of LDA. We have estimated the anisotropic effective masses of electrons and holes of Si(110) for device application.

DOI: 10.1103/PhysRevB.96.125302

I. INTRODUCTION

Over the past ten years, attention has been paid to the Si(110) surface because there are interests in solid state physics and device application as one of the low index surfaces of silicon. For the device application, it is recognized that the Si(110) is a suitable substrate for three-dimensional silicon devices such as FinFETs [1] and Tri-gate FETs [2]. In these 3D devices, the hole mobility of Si(110) surface is 2.4 times larger than that of the Si(100) surface [3], and the electronic states are mainly discussed using empirical tight-binding models and quantum mechanical calculations [4–6]. Surprisingly, there is no experimental data for the electronic band structure of Si(110)-(1×1) surface. It is important to observe the band structure to understand the physical properties and to improve the performance of electronic devices.

Up to now, the electronic states and phonon dispersions of materials have been theoretically investigated mainly by the Kohn-Sham equations [7] with the local-density approximation (LDA) [7–9] or generalized gradient approximation (GGA) [10] for the exchange-correlation energy and potential. However, the applicability of the calculation to real solids has not been sufficiently examined. Recently, Matsushita *et al.* measured the surface phonon dispersion curves of the hydrogen-terminated Si(110)-(1 × 1) [H:Si(110)-(1 × 1)] surface and compared them with the first-principles calculations with LDA [11,12]. While the calculated surface phonon modes agree well with the data in the energy region below 65 meV where bulk phonons exist, a satisfactory agreement between the calculation and the experiment is not seen in the H-Si stretching and bending modes above 65 meV. Shortly afterwards, Tütüncü *et al.* [13] reported that the disagreement is reduced in the GGA calculation. It is therefore interesting to investigate the electronic structure of the H:Si(110)-(1 × 1) surface both with experiment and theory.

The reason why there are no experimental measurements of the electronic structure on the Si(110)-(1 × 1) surface is due to the surface reconstruction. A clean Si(110) surface is reconstructed into Si(110)-(16 × 2) structure [14] with dangling bonds. The surface electronic states were observed while the bulk electronic states behind were not clearly observed [15,16]. We prepared a high quality H:Si(110)-(1 × 1) surface, which is bulk truncated and enables us to observe the electronic structure of intrinsic Si(110) and H-Si bonds at surfaces. Therefore, the H:Si(110)-(1 × 1) surface could be a good template to investigate the electronic band structure of Si(110).

We report here the observation of surface electronic band structure of H:Si(110)-(1 × 1) surface measured by angle-resolved photoemission spectroscopy (ARPES) and compare the experimental results with the calculations using the density functional theory (DFT) with LDA. The surface preparation was carried out with our improved recipe by a wet chemical etching process using NH_4F solution [17–19].

We observed eight electronic bands in ARPES spectra, i.e., one surface state (S_1), seven bulk states (B_1–B_7). The four bulk states (B_1, B_3, B_4, B_5) exhibit anisotropic band dispersions along the high symmetric direction of $\overline{\Gamma}$-$\overline{X}$ and $\overline{\Gamma}$-$\overline{X}'$ directions. Intriguingly, one of them (B_4) shows one-dimensional band dispersion, reflecting the anisotropic atomic structure of the surface. The surface state has its origin in the H-Si bonds on the surface and shows a two-dimensional band dispersion, indicating the existence of the H-H interaction between the nearest neighbor H atoms. We have investigated the physical properties and the origin of these electronic states by comparing them with the calculations. We also discuss the anisotropic effective masses of Si(110) based on the electronic band structure.

*Present address: Department of Physics, University of Tokyo, Tokyo 113-003, Japan.

†Present address: AdvanceSoft Corp., Tokyo 101-0062, Japan.

‡Corresponding author: suto@surface.phys.tohoku.ac.jp

 ©2017 American Physical Society

II. EXPERIMENTS AND CALCULATIONS

A sample for ARPES measurements ($15 \times 3 \times 1$ mm^3) was cut out from a commercial *n*-type Si(110) wafer (P doped, <0.02 Ω cm, SUMCO, Japan). H:Si(110)-(1 × 1) was done by a wet chemical process with an etching solution containing 40% w/w of NH_4F (Morita Chemical, Japan) and 1.0% w/w of $(NH_4)_2SO_3$ (Kanto Chemical Co., Japan). Details of preparation procedures were described in Refs. [17–19].

ARPES measurements were performed with a MBS A-1 spectrometer equipped with xenon and helium discharge lamps [20,21]. We used the Xe Iα ($h\nu = 8.437$ eV), He Iα (21.2 eV), and He IIα (40.8 eV) lines to excite photoelectrons. We measured ARPES spectra along the two high-symmetry lines of $\overline{\Gamma}$-$\overline{X}$ and $\overline{\Gamma}$-$\overline{X}'$ in the Brillouin zone of the H:Si(110)-(1 × 1) surface. The sample orientation was determined by low-energy electron diffraction (LEED) measurement. The energy and angular resolutions were set at 20 meV and 0.1°, respectively. The sample was kept at 100 K during the measurements. The Fermi level (E_F) of the sample was referenced to that of a gold film evaporated onto the sample holder. We also carried out scanning tunneling microscope (STM) measurements to confirm the lattice constants and quality of the H:Si(110)-(1 × 1) surface.

In order to analyze the ARPES data, we carried out DFT [7,22] calculations using ABINIT code [23] within the framework of plane-wave and norm-conserving pseudopotential method [24]. Clean and H-terminated Si(110)-(1 × 1) surfaces were represented by slab models having 11, 21, and 31 Si layers and a vacuum region with a thickness of about 15 Å. The kinetic energy cutoff for plane-wave basis sets was 15 Ha. The number of $\boldsymbol{k}$-point sampling was $8 \times 8 \times 1$ for the slab calculations. All calculations were done using LDA functional [25] for exchange-correlation energy and potential. Theoretical lattice constant of Si bulk was 5.398 Å [12], which was used for constructing the slabs. The structure optimization was carried out for the slabs until all the forces acting on the atoms were smaller than 5.0×10^{-5} Ha/bohr. Unless otherwise specified, the results of slab calculation with 11 Si layers are shown in figures and tables.

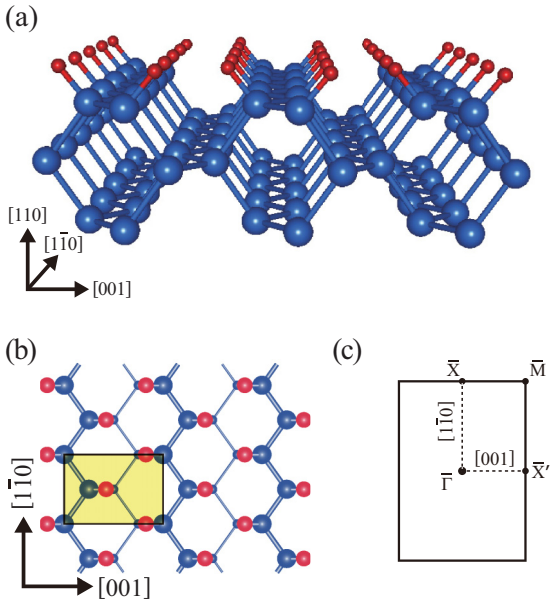

FIG. 1. (a) A bird's-eye view and (b) top view of H:Si(110)-(1 × 1) surface. The red and blue spheres represent H and Si atoms, respectively. The yellow area in (b) shows the rectangular Bravais lattice of a *p2mg* two-dimensional space group. (c) Schematic drawing of the associated first surface Brillouin zone and the two highly symmetric directions of $\overline{\Gamma}$-$\overline{X}$ and $\overline{\Gamma}$-$\overline{X}'$.

III. RESULTS

A. Structure and ARPES spectra along $\overline{\Gamma}$-$\overline{X}$ and $\overline{\Gamma}$-$\overline{X}'$ directions

Figure 1 shows the crystal structure of H:Si(110)-(1 × 1) surface and the first surface Brillouin zone (SBZ). ARPES spectra were recorded along the two high-symmetry lines of $\overline{\Gamma}$-$\overline{X}$ and $\overline{\Gamma}$-$\overline{X}'$. The distances of $\overline{\Gamma}$-$\overline{X}$ and $\overline{\Gamma}$-$\overline{X}'$ are 0.82 Å^{-1} and 0.58 Å^{-1}, respectively. The surface morphology and the atomic structure of the sample were checked by LEED and STM as shown in Fig. 2. The LEED pattern shows clear *p2mg* space group in Fig. 2(a), and the STM images indicate the step and terrace structure extended in $\overline{\Gamma}$-$\overline{X}$ direction in Figs. 2(b) and 2(c) [18]. Furthermore, the atomic image of H atoms are clearly observed in Fig. 2(c). The streaks at 01 and 0$\bar{1}$ spots in Fig. 2(a) are due to the step and terrace structure along the [001] direction as shown in Figs. 2(b) and 2(c). We reported the relation between the coherence length of electron beams and terrace widths in Ref. [18]. These results

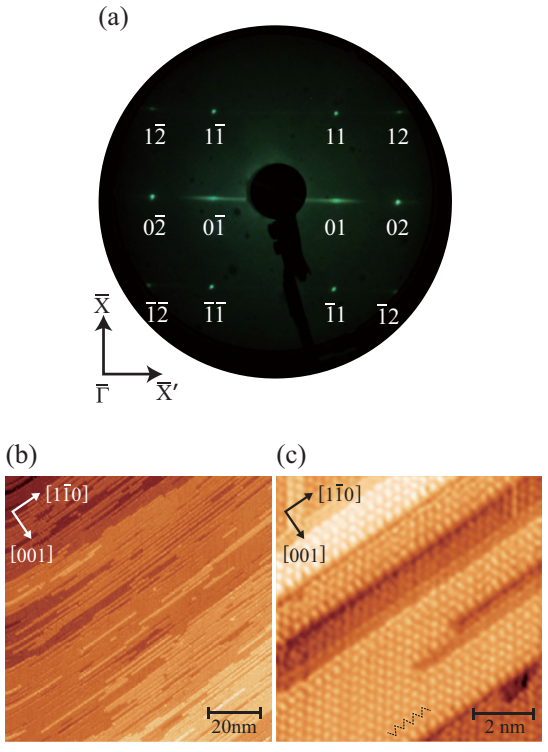

FIG. 2. (a) LEED pattern of H:Si(110)-(1 × 1) surface. The incident electron beam energy is 70 eV. (b) Large scale STM image of H:Si(110)-(1 × 1) surface. The image area is 100 × 100 nm^2. The bias voltage is −1.8 V and the current is 140 pA. (c) Atomic scale STM image of H:Si(110)-(1 × 1) surface. The image area is 8×8 nm^2. The bias voltage is −2.1 V and the current is 190 pA.

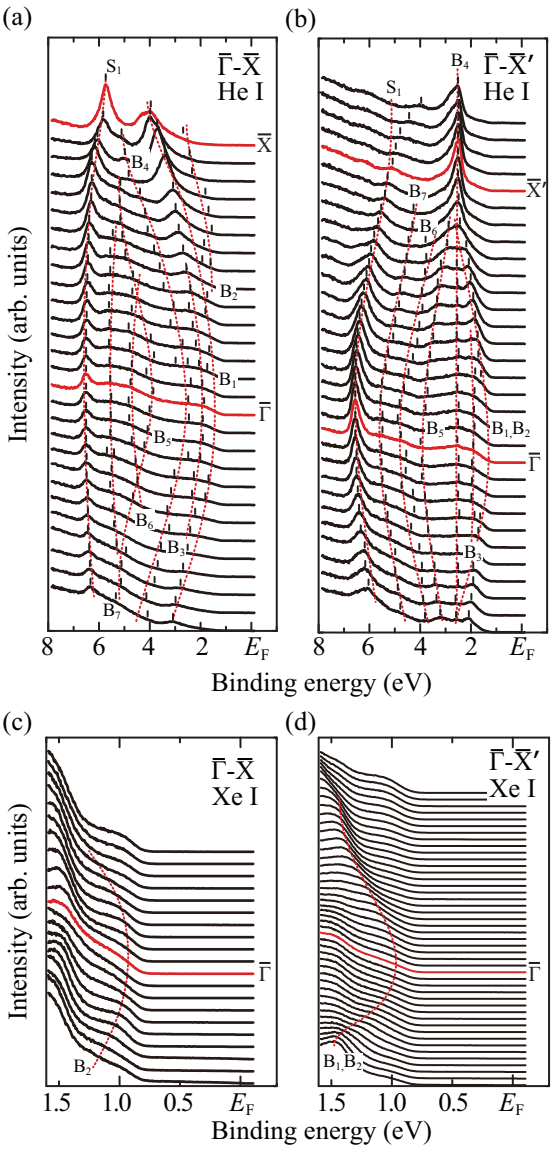

FIG. 3. Sets of angle-resolved photoemission spectra of Si(110) surface recorded for different polar angles: (a) along $\overline{\Gamma}$-$\overline{X}$ and (b) along $\overline{\Gamma}$-$\overline{X}'$ directions measured by He Iα, (c) along $\overline{\Gamma}$-$\overline{X}$, and (d) along $\overline{\Gamma}$-$\overline{X}'$ directions measured by Xe Iα. The EDCs in red lines represent the spectra at $\overline{\Gamma}$, $\overline{X}$, and $\overline{X}'$ points. The vertical bars in (a) and (b) are the peak positions estimated by second derivative of EDC, and the red dashed lines are curves fitted using cosine functions.

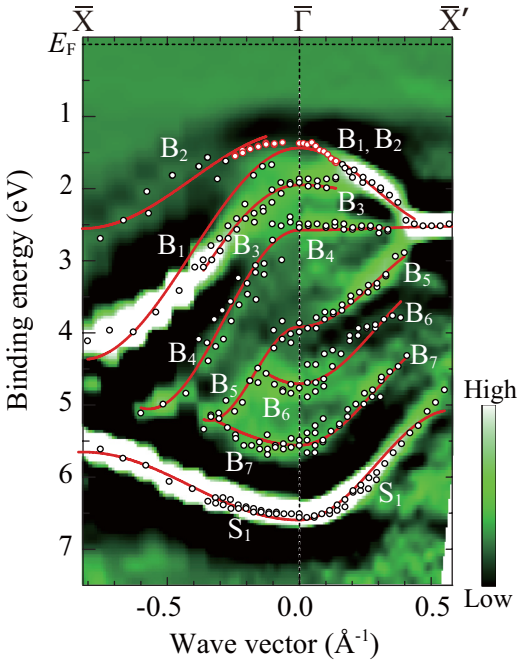

FIG. 4. The second derivative photoemission intensity map of H:Si(110)-(1 × 1) surface measured by He Iα line. The black and red open circles are the peaks shown in Figs. 3(a) and 3(b) and Figs. 3(c) and 3(d), respectively. The red lines are the band dispersion of each electronic state obtained from curve fitting using cosine functions.

confirmed the H-truncated surface is equivalent to the intrinsic unreconstructed surface and that the quality of samples is high enough to measure dispersion curves by ARPES.

Figures 3(a) and 3(b) show the energy distribution curves (EDCs) of the H:Si(110)-(1 × 1) surface along the $\overline{\Gamma}$-$\overline{X}$ and $\overline{\Gamma}$-$\overline{X}'$ lines, respectively, measured with He Iα photons. Peaks and shoulders identified by second derivative of spectra are indicated by black bars. Details of how to read peak positions and shoulders are shown in the Supplemental Material [26]. We observed eight bands in the $\overline{\Gamma}$-$\overline{X}$ direction while seven bands are resolved in the $\overline{\Gamma}$-$\overline{X}'$ direction. We labeled these bands as B_1–B_7 and S_1 as shown in Figs. 3(a) and 3(b). All the bands are commonly observed in both $\overline{\Gamma}$-$\overline{X}$ and $\overline{\Gamma}$-$\overline{X}'$, where B_1 and B_2 bands overlap in the $\overline{\Gamma}$-$\overline{X}'$ direction. Figures 3(c) and 3(d) show the EDCs measured with the Xe Iα line. It is remarked that the dispersion of B_2 band is only observed in the $\overline{\Gamma}$-$\overline{X}$ direction, while the band dispersion of B_1 and B_2 bands are observed in the $\overline{\Gamma}$-$\overline{X}'$ direction. The details in the band assignments are discussed in the next subsection.

The present ARPES results in Fig. 3 clearly show that there are no bands at the Fermi level (E_F). This shows a sharp contrast with a previous report that several metallic states due to the dangling bonds appear on Si(110)-(16 × 2) [15,16] as well as a theoretical prediction that clean Si(110)-(1 × 1) surface is metallic [27]. The disappearance of these dangling-bond states in our sample indicates that the hydrogen termination is perfectly done in the present sample, leading to formation of an ideal H:Si(110)-(1 × 1) surface.

B. Dispersion along $\overline{\Gamma}$-$\overline{X}$ and $\overline{\Gamma}$-$\overline{X}'$ directions

Figure 4 shows the band dispersion of H:Si(110)-(1 × 1) surface along $\overline{\Gamma}$-$\overline{X}$ and $\overline{\Gamma}$-$\overline{X}'$ directions. Red and black open circles denote the experimental data, and red lines indicate the fittings to the experimental results for each band using cosine functions. Table I summarizes the binding energy at $\overline{\Gamma}$ point for each band and the band width along $\overline{\Gamma}$-$\overline{X}$ and $\overline{\Gamma}$-$\overline{X}'$ directions. We classified the eight bands into three groups according to their intensities and dispersive features: The B_1, B_3, B_4, and B_5 bands have highly anisotropic band dispersions along $\overline{\Gamma}$-$\overline{X}$ and $\overline{\Gamma}$-$\overline{X}'$ directions, while the B_2, B_6, and B_7 bands have almost isotropic band dispersions and the intensities are relatively weak. The S_1 band has the strongest intensity all over the Brillouin zone.

TABLE I. Binding energies and band widths at $\overline{\Gamma}$ point. The energy of B_4 band at $\overline{\Gamma}$ calculated by DFT is given with the corresponding experimental data.

	Energy at $\overline{\Gamma}$		ΔE	
	Experiment	DFT	$[1\bar{1}0]$	[001]
B_1	1.4	1.3	2.8	1.1
B_2	1.4	1.5	1.3	1.1
B_3	1.9	1.8	1.2	0.1
B_4	2.5	2.5	2.6	0.0
B_5	3.9	4.1	1.5	−1.0
B_6	4.8	4.3	−0.2	−1.0
B_7	5.6	5.4	−0.4	−1.2
S_1	6.6	5.9	−1.1	−1.8

At the $\overline{\Gamma}$ point, the B_1, B_3, B_4, and B_5 bands are observed at 1.4, 1.9, 2.5, and 3.9 eV, respectively. The B_1 and B_3 bands show downward dispersions in both directions, while these bandwidths are considerably smaller in the $\overline{\Gamma}$-$\overline{X}'$ direction than in the $\overline{\Gamma}$-$\overline{X}$ direction, as shown in Table I. On the other hand, the band B_5 shows a totally anisotropic band dispersion; it is downward in $\overline{\Gamma}$-$\overline{X}([1\bar{1}0])$ direction while it is upward in $\overline{\Gamma}$-$\overline{X}'([001])$. It is remarked that the B_4 band is almost dispersionless in $\overline{\Gamma}$-$\overline{X}'$ direction while it shows a downward dispersion in $\overline{\Gamma}$-$\overline{X}$ direction.

The B_6 and B_7 bands are observed at 4.8 and 5.6 eV, respectively, at the $\overline{\Gamma}$ point. The top of B_2 band is located at 1.4 eV near the $\overline{\Gamma}$ point. The B_2 band shows a downward dispersion in both $\overline{\Gamma}$-$\overline{X}$ and $\overline{\Gamma}$-$\overline{X}'$ directions and overlap with B_1 band in the $\overline{\Gamma}$-$\overline{X}'$ direction. The B_6 and B_7 bands show upward dispersions. The intensities of these three bands are very weak all over the Brillouin zone, compared with the B_1, B_3, B_4, B_5, and S_1 bands. The S_1 band with the strongest intensity is observed at 6.6 eV at the $\overline{\Gamma}$ point and shows an upward dispersion in both $\overline{\Gamma}$-$\overline{X}$ and $\overline{\Gamma}$-$\overline{X}'$ directions.

C. Photon-energy dependence of ARPES spectra of H:Si(110)-(1 × 1) surface

Figure 5 shows the photoemission spectra measured by He Iα (21.2 eV) and He IIα (40.8 eV) measured at the $\overline{\Gamma}$ point and $k = 0.37$ Å^{-1} in the $\overline{\Gamma}$-$\overline{X}'$ direction. In the spectra at the $\overline{\Gamma}$ point, two peaks of B_4 and S_1 bands, and three shoulders of B_3, B_5, and B_6 bands, are observed. Since the B_3, B_4, and S_1 bands show no energy shift between He Iα to He IIα excitations, S_1 bands is surface origin. Later, we assign the B_3 and B_4 bands to bulk states of $3p_{xy}$ orbitals as will be discussed with Fig. 8. The S_1 band is assigned to a surface state. The change of spectral intensity of each band is due to the difference in the cross section between He Iα and He IIα [28]. It is noteworthy that the peak position of B_4 band is independent both of the incident-photon-energy and the wave vector along the $\overline{\Gamma}$-$\overline{X}'$ direction, indicating that the B_4 band is a one-dimensional electronic state.

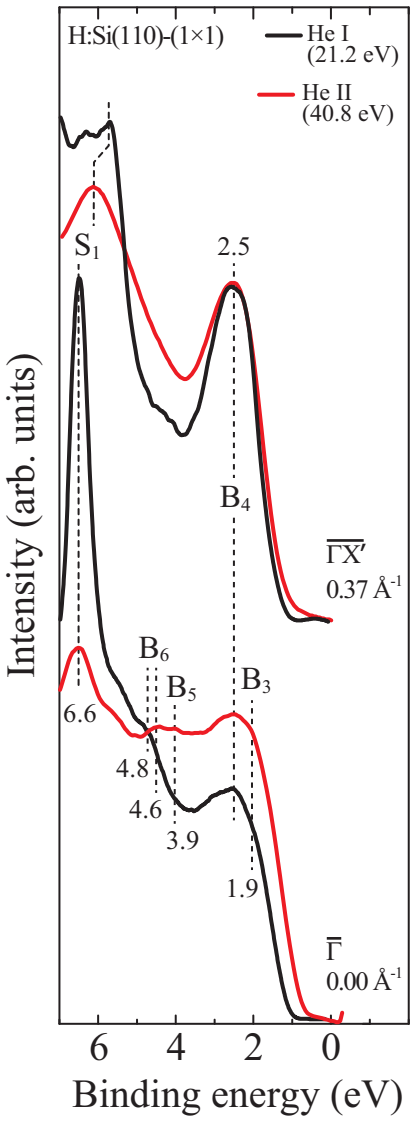

FIG. 5. The incident energy dependence of ARPES spectra of H:Si(110)-(1 × 1) surface. The light sources are He Iα (21.2 eV) and He IIα (40.8 eV), which are represented by black and red lines, respectively. The spectra are measured at $\overline{\Gamma}$ point and at 0.37 Å^{-1} along $\overline{\Gamma}$-$\overline{X}'$, respectively.

IV. DISCUSSION

A. Comparison of experimental results with DFT calculation

Figure 6 shows the theoretical electronic band structure of H:Si(110)-(1 × 1) surface calculated by DFT. The energy was measured from the valence band maximum (VBM) which corresponds to the binding energy of 1.4 eV in the ARPES results. More specifically, we aligned the calculated B_4 band at $\overline{\Gamma}$ with the corresponding experimental data. The solid lines are the surface band dispersion curves obtained from the slab calculation, which represent the quantization of the bulk states due to the limited extension of the slab. The blue, green, red, and yellow regions exhibit the states made from Si $3s$, Si $3p_z$, Si $3p_{xy}$, and Si $3p_{xy} + 3p_z$, respectively. Here, we defined the electronic wave functions of Si as $3p_{xy}$ and $3p_z$, where $3p_{xy}$ is the $3p$ orbital of Si-Si bonds lie in the Si(110) plane (the bond

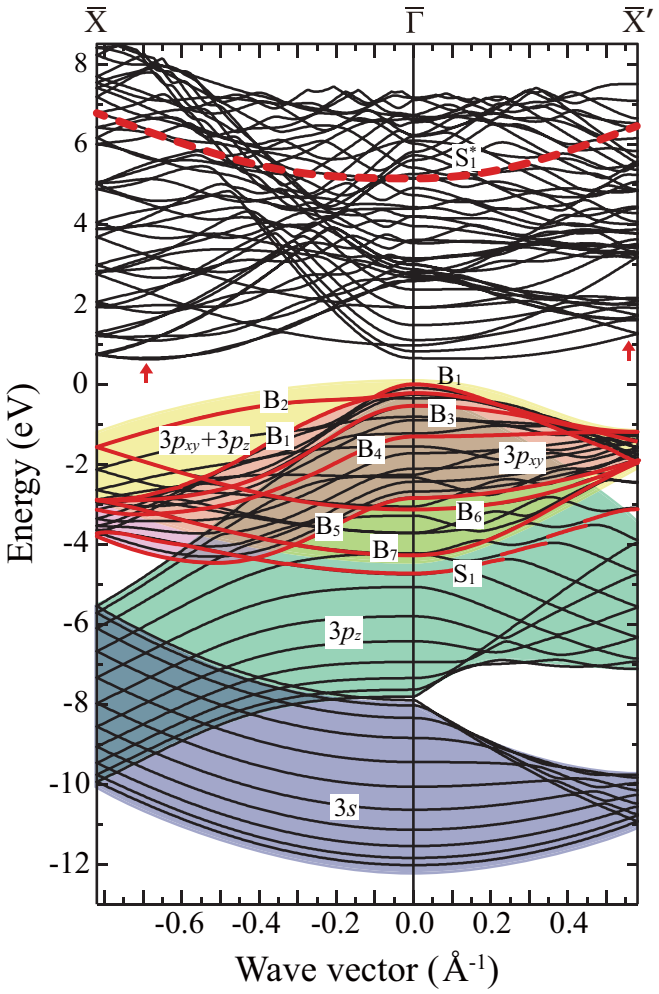

FIG. 6. The electronic band structure of H:Si(110)-(1 × 1) surface calculated by first-principles calculations of density-functional theory. The background is the surface projection of bulk Si, where blue, green, red, and yellow regions exhibit the states made from Si 3s, Si 3p_z, Si 3p_{xy}, and Si 3p_{xy} + 3p_z, respectively. The red lines show the bands used for analysis of experimental data. The red dashed line indicates the unoccupied surface state, which is located at 5.2 eV at $\overline{\Gamma}$ and has the same orbital character as the occupied surface state(S_1), i.e., H 1s + Si 3p_z. The two red arrows indicate the positions of valley in the conduction bands which are discussed in the text.

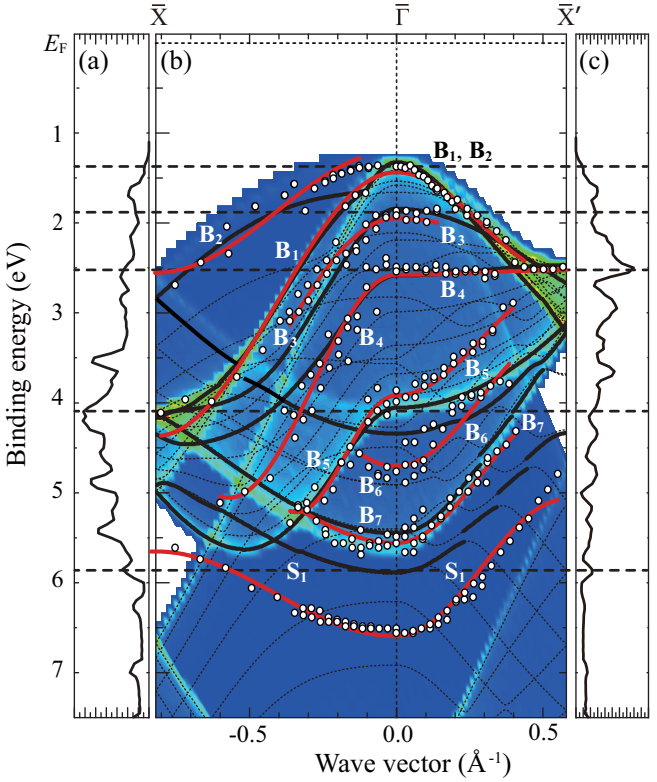

FIG. 7. The calculated density of sates of H:Si(110)-(1 × 1) surface along (a) $\overline{\Gamma}$-$\overline{X}$ and (c) $\overline{\Gamma}$-$\overline{X}'$. (b) the experimental and calculated band structures of H:Si(110)-(1×1) surface along the two highly symmetric directions $\overline{\Gamma}$-$\overline{X}$ and $\overline{\Gamma}$-$\overline{X}'$. The experimental data are shown as open circles and the red lines are the fitting curves as shown in Fig. 4. The thin dotted lines are the calculated energy bands and the thick black lines indicate the calculated bands corresponding to our observation. The blue region denotes the calculated surface projected bulk energy bands. In order to compare the calculation with the experimental results, the energy of B_4 bands at $\overline{\Gamma}$ is aligned.

which forms the Si-Si zigzag chain on the surface), and 3p_z is the 3p orbital of Si-Si bonds perpendicular to the (110) plane.

The dispersion curves of four characteristic bands from top to bottom, which are related to our experimental results, are indicated by red lines: The first one (B_1) is the curve lying in the VBM and the top of 3p_{xy} state, which shows a highly anisotropic band dispersion in $\overline{\Gamma}$-$\overline{X}$ and $\overline{\Gamma}$-$\overline{X}'$ directions. The second one (B_4) is a one-dimensional dispersion curve of which dispersion is almost flat in $\overline{\Gamma}$-$\overline{X}'$ direction. Third one (B_5) shows the boundary of the bottom of the electronic states made of the 3p_{xy} orbital. The fourth one (S_1) lying at around −4.5 eV is the two-dimensional surface state of H-Si bonds. Furthermore, we calculated the electronic structure of clean Si(110)-(1×1) surface as shown in the Supplemental Material and confirmed the two-dimensional surface state of H-Si bonds [26].

Figure 7 shows the experimental data, calculated band structure, and the density of states in $\overline{\Gamma}$-$\overline{X}$ and $\overline{\Gamma}$-$\overline{X}'$ directions. In Fig. 7(b), the open circles denote the experimental data and red lines exhibit the experimental dispersion curves obtained by curve fitting using cosine functions as shown in Fig. 4. The thin dotted black lines are the calculated dispersion curves as shown in Fig. 6 and black solid lines are the theoretical dispersion curves corresponding to the experimental curves. Figures 7(a) and 7(c) indicate the density of states in $\overline{\Gamma}$-$\overline{X}$ and $\overline{\Gamma}$-$\overline{X}'$ directions, respectively. Here, in order to compare the experiment and the theory, the B_4 band was aligned, because the highest density of states is observed experimentally and theoretically as shown in Fig. 7(c). The background of Fig. 7(b) is the continuum of Si bulk states projected along the (110) direction onto the SBZ. We present the projection as a colored map, which reflects the density of quasiparticle bulk states of k points in the bulk Brillouin zone, to highlight the high density of bulk states in the continuum. It is found that the experiment and the theory agree well, except the S_1 band. There are also deviations of B_4 and B_5 bands in the high wave-vector side

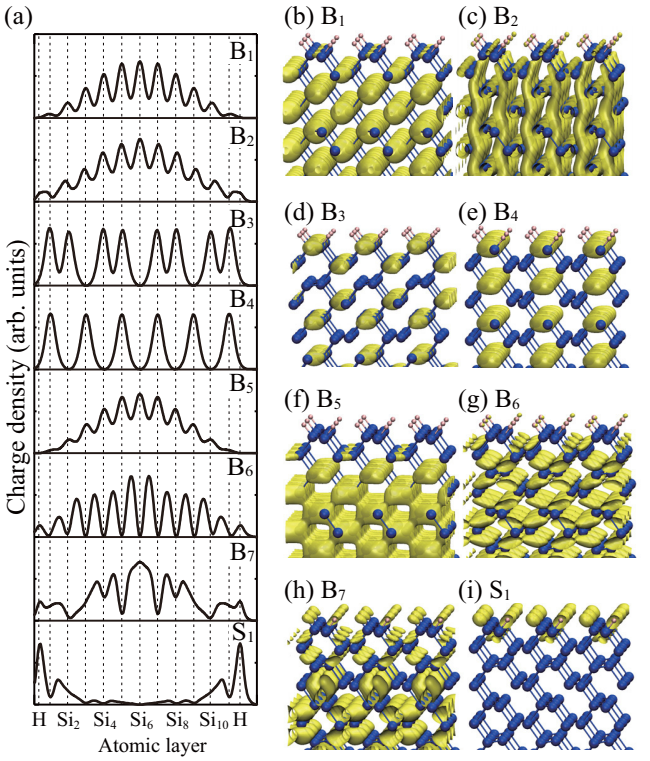

FIG. 8. (a) Laterally averaged charge density profiles at the $\overline{\Gamma}$ point normal to the surface. (b)–(i) Charge density profiles of characteristic electronic states at the $\overline{\Gamma}$ point. The red and blue spheres indicate H and Si atoms, respectively, and the yellow clouds show the iso-charge-density surface.

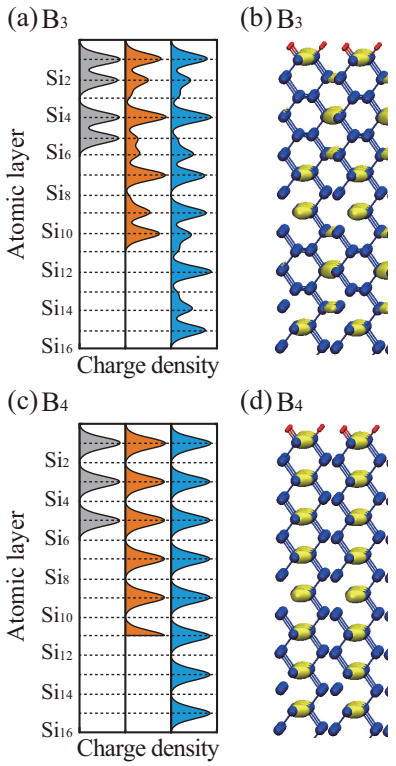

FIG. 9. Slab thickness dependence of charge density profiles of B_3 and B_4 states at the $\overline{\Gamma}$ point normal to the surface. (a) and (c): the slab thickness of 11 Si layers (gray), 21 Si layers (orange), and 31 Si layers (blue) terminated by H atoms, respectively. (b) and (d): three-dimensional drawing of isocharge density surfaces for the slab of 31 Si layers as shown by yellow clouds. The red and blue spheres indicate H and Si atoms, respectively.

due to the mixing of other states. Furthermore, we calculated energy bands of H:Si(110)-(1 × 1) surfaces for slab thickness of 21 Si layers and 31 Si layers terminated with H atoms at both surfaces to confirm the reliability of the energy band calculations [26].

Here, we discuss the band structure whose origin is the intrinsic Si(110)-(1 × 1) surface with the help of charge density profiles as shown in Figs. 8–10. First, we discuss the nature of each state from the charge density profile in the direction normal to the surface shown in Fig. 8(a). In general, there are three possible energy states, i.e., surface states, surface resonant bulk states, and bulk states [29]. As shown in Fig. 8(a), the S_1 state shows the typical surface state where the charge density at the surfaces is very large. In contrast, the B_1, B_2, B_5, B_6, and B_7 states indicate the typical bulk state where the charge density is large at the center of the slab and very small at the surfaces. The charge density profiles of B_3 and B_4 states in Fig. 8(a) show uniform profile whole through the 11 Si layers.

In order to elucidate the nature of B_3 and B_4 states, we further performed the DFT calculation for slab thickness of 21 Si layers and 31 Si layers terminated with H atoms at both surfaces. Figure 9 shows the thickness dependence of charge density profiles of B_3 and B_4 states. For the B_3 state, the profile changes with slab thickness from 11 Si layers to 21 Si layers and no change from 21 Si layers to 31 Si layers. However, the band structure of B_3 state changes very little, which was discussed in the Supplemental Material [26]. For the B_4 state, there is no thickness dependence. In three thicknesses, the charge density distributes in the odd number layers and uniformly spreads throughout the slab. Therefore, we assigned the B_3 and B_4 states to bulk bands of $3p_{xy}$ orbital. There is no surface resonant bulk state.

Second, we discuss the nature of B_x ($x = 1, 3, 4, 5$) bands composed of the $3p_{xy}$ orbital in the direction parallel to the surface. Figures 8(b), 8(d)–8(f) show that the charge densities localize in the Si-Si bond, which forms the zigzag chain structure of Si(110)-(1 × 1) surface along the $[1\bar{1}0]$ direction, and are very weakly connected to the [110] direction, i.e., surface normal direction. Therefore, the dispersion of B_x ($x = 1, 3, 4, 5$) bands are highly anisotropic in $\overline{\Gamma}$-$\overline{X}$ and $\overline{\Gamma}$-$\overline{X}'$ directions. These bands are made of $3p_{xy}$ orbital and show very weak k_z dependence. This is the reason why we observed the same energies with different photon energies as shown in Fig. 5.

Third, we discuss the nature of one-dimensional B_4 band. In each (110) layer, the electronic charge is continuous along the $[1\bar{1}0]$ direction, i.e., $\overline{\Gamma}$-$\overline{X}$ direction, while it is separate along the [001] direction. Intriguingly, the B_4 band shows one-dimensional dispersion in Fig. 7(b) and the electronic charge profile also shows the one-dimensional property. The charge exists only in the odd layers. Therefore, the electrons are confined into the individual Si-Si chain and propagate only along $[1\bar{1}0]$ direction, making the B_4 band one dimensional.

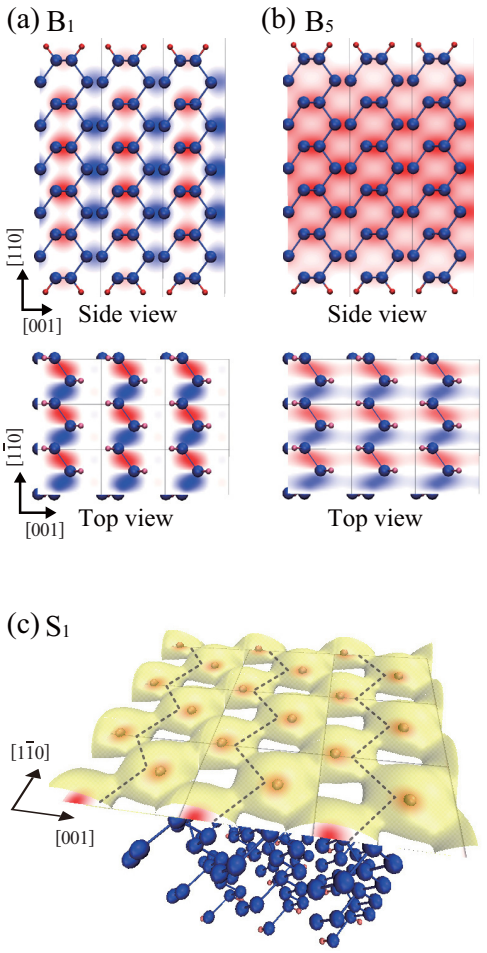

FIG. 10. (a) and (b) show the wave functions of B_1 and B_5 states, respectively. The red and blue spheres indicate H and Si atoms, respectively, and the red and blue regions indicate the positive and negative phase of electronic wave functions, respectively. (c) The light yellow cloud indicates iso-charge-density surface of S_1 state. The cross section is drawn at the center of H atoms, parallel to the (110) surface. The dashed lines indicate the Si-Si chains of the first Si layer. The real part of wave functions and charge density profiles are chosen at the $\overline{\Gamma}$ point.

Fourth, we discuss the dispersion of B_1 and B_5 bands. The B_1 and B_5 bands are observed because the two states are located at the top and bottom of the $3p_{xy}$ states where are the onset of density of states as shown in Fig. 7. The B_1 band shows downward dispersion in $\overline{\Gamma}$-$\overline{X}$ and $\overline{\Gamma}$-$\overline{X}'$ directions, while the B_5 band shows downward dispersion in the $\overline{\Gamma}$-$\overline{X}$ direction and upward dispersion in the $\overline{\Gamma}$-$\overline{X}'$ direction. These results are compatible with those on the level densities of B_1 and B_5 shown in Figs. 10(a) and 10(b), because the dispersion curve shows upward (downward) dispersion when the sign of wave function in the neighbors is the same (different) for B_5 (B_1).

Fifth, the charge density of B_x ($x = 2,6,7$) bands spread not only in Si-Si bond in the (110) plane but also perpendicular to the (110) plane, i.e., [110] direction. Therefore, we assigned the B_x bands to the bulk states. B_2 band has the component of $3p_{xy}$ and $3p_z$, while B_6 and B_7 have only the component of $3p_z$ as shown in Figs. 8(c), 8(g) and 8(h). The existence of $3p_z$ component may cause a weak surface localization of B_2, B_6, and B_7 bands compared to the B_1, B_3, B_4, and B_5 bands, which corresponds to the weak intensity of B_2, B_6, and B_7 bands in the ARPES measurement.

Kim *et al.* observed the bulk band in the $\overline{\Gamma}$-$\overline{X}'$ direction on the Si(110)-(16 × 2) surface, which coincides with the upper band edge of $3p_z$ orbitals [15]. We believe that we didn't observe it due to the difference in incident energy.

Finally, the origin of S_1 band is the H-Si bond on the H:Si(110)-(1 × 1) surface. The charge distribution of this state is strongly localized at the H atoms on the surface and the first layer of Si atoms, whose origin is the $1s$ orbital of H atom and $3p_z$ orbital of Si atom. The strong intensity in the ARPES measurement is due to the strong surface localization of this state. Therefore, we assigned the S_1 band to the surface state. Note that the S_1 band is dispersive in both $\overline{\Gamma}$-$\overline{X}$ and $\overline{\Gamma}$-$\overline{X}'$ directions, indicating the existence of two-dimensional interaction between the H-Si bonds on the H:Si(110)-(1 × 1) surface as shown in Fig. 10(c).

The dispersion curve of S_1 band in the DFT calculation shows a redshift of 0.7 eV from the experimental result at $\overline{\Gamma}$, while the curvature of the band agrees well with the experiment. The charge density distribution at the interface of the H-Si surface and vacuum rapidly varies. The LDA is probably the main cause because the S_1 state is localized at the surface that is treated by GGA more properly than LDA. Such an energy deviation was reported also in the surface phonon dispersion of H:Si(110)-(1 × 1) surface [11,12]. Recently, Tütüncü *et al.* reported that this deviation is improved by using GGA calculation [13]. The same strategy could be applied to the electronic band structure to understand the discrepancy in the S_1 band between the calculation and the experiments.

Hricovini *et al.* observed the surface state of H-Si bonds at 5.8 eV below E_F near the K point in H:Si(111) surface [30]. Gallego *et al.* identified the origin of this state to H $1s$ and Si $3p$ orbital using polarization-dependent ARPES [31]. He *et al.* observed seven bulk states and the surface state of H-Si bonds for the H:Si(111) surface [32]. The top of the valence band is located at 1.4 eV below E_F. Their surface state showed no dispersion, because there is no sizable interaction between H atoms. The nearest neighbor distance of H-H is 0.299 nm on H:Si(110)-(1 × 1) surface, while the distance is 0.384 nm on H:Si(111)-(1 × 1) surface [12,18].

Sakamoto *et al.* observed the weak and dispersion less bands within the projected bulk band on the Si(110)-(16 × 2) surface, which are quite different from our observation [16]. The dispersion less band structure is considered to be the folding effect of 16 × 2 surface reconstruction. Besides, photoelectrons could be affected by the umklapp processes or diffraction effect due to the 16 × 2 structure [33]. By keeping the 1 × 1 structure of H:Si(110) surface, we are able to observe the intrinsic band structure of Si(110) without these effects.

B. Estimation of electronic mobility of Si(110) surface

The effective masses of holes were estimated by parabolic curve fittings of both B_1 and B_2 bands around the $\overline{\Gamma}$ point. Since the two bands are overlapped in the $\overline{\Gamma}$-$\overline{X}'$ direction, the effective mass is 0.33 m_e (m_e is the free electron mass). In the $\overline{\Gamma}$-$\overline{X}$ direction, on the other hand, that of B_1 band exhibits

TABLE II. Effective masses of holes and electrons of H:Si(110)-(1 × 1) for both B_1 and B_2 bands around the $\overline{\Gamma}$ point. The unit of mass is mass of free electron (m_e).

	$[1\bar{1}0]$	[001]	$m_{[001]}/m_{[1\bar{1}0]}$
Holes			
Expt.	0.23	0.33	1.4
DFT	0.12	0.32	2.7
[Parabolic]	0.23	0.33	1.4
[Polynomial]	0.15	0.39	2.6
Electrons			
DFT	0.62	0.73	1.2

0.23 m_e while B_2 band has 0.99 m_e. We use the light effective mass for conductivity as shown in Table II. The ratio of effective masses between the two directions ($m_{001}/m_{1\bar{1}0}$) is 1.4 in the experiment, while it is 2.7 in the DFT calculation.

In order to verify the accuracy of band fitting, the effective masses were also estimated from the polynomial curve fitting with up to the fourth order term. In the case of polynomial fitting, the effective mass in the $\overline{\Gamma}$-$\overline{X}'$ direction is 0.39 m_e, and that in the $\overline{\Gamma}$-$\overline{X}$ direction is 0.15 m_e and 1.13 m_e for B_1 and B_2, respectively.

In the case of conduction band, the valley structures far from the $\overline{\Gamma}$ point, shown by red arrows in Fig. 6, dominate the electronic transport [6]. Because of the lack of experimental data for the conduction band, we estimated the electron effective masses with the DFT calculation. We carried out the parabolic band fitting to the two valleys in $\overline{\Gamma}$-$\overline{X}$ and $\overline{\Gamma}$-$\overline{X}'$ directions and calculated the effective masses for each direction. The electron effective masses are 0.62 m_e in $\overline{\Gamma}$-$\overline{X}$ and 0.73 m_e in $\overline{\Gamma}$-$\overline{X}'$ directions, and the ratio $m_{001}/m_{1\bar{1}0} = 1.2$. The estimated values are summarized in Table II.

The effective mass and mobility in the free electron Fermi gas are related with $\mu = e\tau/m^*$, where τ is the relaxation time. Assuming that τ is independent of the channel direction, we obtain the relationship of $\frac{\mu_{1\bar{1}0}}{\mu_{001}} = \frac{m_{001}}{m_{1\bar{1}0}}$. According to the carrier mobility measurements in the previous works, they obtain the ratio of hole carrier as 1.3 [34] and electron carrier as 0.8 [35]. The effective mass ratio of hole carrier is consistent with our estimation, indicating that the anisotropy of carrier transport of p-type devices can be explained by the atomic structure of Si(110) surface. On the other hand, the effective mass of n-type devices is larger along $[1\bar{1}0]$ than [001], which is opposite to the band structure. To understand this inconsistency, we have to consider the quantum mechanical confinement and the phonon scattering between the sublevels [4–6].

V. CONCLUSION

We investigated the electronic band structure of H:Si(110)-(1 × 1) surface using ARPES and DFT calculations and assigned the intrinsic band structure of Si(110) and the surface state due to the H-Si bond. We successfully observed intrinsic electronic structure of Si(110) without the influence of 16 × 2 surface reconstruction. Furthermore, the effective masses of the electrons and holes of Si(110) were estimated. We also discussed the applicability of LDA to semiconductor surfaces.

In ARPES experiments, we observed eight electronic bands, consisting of seven bulk states (B_1–B_7) and one surface state (S_1). We clarified the atomic orbitals and the curvature of the detected bands by comparing the experimental results with DFT calculation and found that the seven bulk bands are attributed to the intrinsic Si(110) and the surface state is due to the H-Si bond. The observed band structure of bulk states agrees well with the theoretical calculations, but the observed energy of the surface state is lower than the calculated one at $\overline{\Gamma}$. The main cause of the deviation is probably the LDA that in general does not well represent the abrupt charge density change at the surface region.

In the top region of the valence band, there are four bulk bands, whose dispersion curves are highly anisotropic in $\overline{\Gamma}$-$\overline{X}$ and $\overline{\Gamma}$-$\overline{X}'$ directions. The states are made of the $3p_{xy}$ orbitals of Si bonds and reflect the zigzag chain structure of the Si(110) surface. In particular, B_4 band shows a one-dimensional character, where electrons are confined into the individual chains and propagate only along $\overline{\Gamma}$-$\overline{X}$ direction (parallel to the chain). The surface state of H-Si bonds (S_1 band) is strongly localized in the top layer of the surface, and shows a two-dimensional energy dispersion in $\overline{\Gamma}$-$\overline{X}$ and $\overline{\Gamma}$-$\overline{X}'$ directions. According to the charge density profile calculated by DFT, we found that this dispersion is due to the direct H-H interaction of the nearest neighbor H atoms.

We have estimated the effective masses of holes to be 0.23 m_e and 0.33 m_e in $\overline{\Gamma}$-$\overline{X}$ and $\overline{\Gamma}$-$\overline{X}'$ directions, respectively. The electron effective masses obtained from the DFT calculation are 0.62 m_e in $\overline{\Gamma}$-$\overline{X}$ and 0.73 m_e in $\overline{\Gamma}$-$\overline{X}'$ directions. The effective mass ratio of the valence band ($m_{001}/m_{1\bar{1}0} = 1.4$) is very close to that of p-type MOSFET of 1.2, indicating that the anisotropic transport of holes is due to the anisotropic chain structure of the Si(110) surface.

ACKNOWLEDGMENTS

We would like to thank T. Sato, J. Kang, T. Yamada, T. Wakita, K. Haga, and H. Kato for useful discussions. This work was partially supported by the Grant-in-Aid for Scientific Research from the Ministry of Education, Culture, Sports, Science and Technology (MEXT) and by Global COE Program "Weaving Science Web beyond Particle-Matter Hierarchy" from MEXT. S.Y.M. and E.K. also thank the Tohoku University Institute for International Advanced Research and Education for their financial support.

[1] Y.-K. Choi, T.-J. King, and C. Hu, IEEE Electron Device Lett. **23**, 25 (2002).

[2] M. Saitoh, Y. Nakabayashi, K. Uchida, and T. Numata, IEEE Electron Device Lett. **32**, 273 (2011).

[3] S. Sugawa, I. Ohshima, H. Ishino, Y. Saito, M. Hirayama, and T. Ohmi, in *Proceedings of the IEEE International Electron Devices Meeting Technical Digest* (IEEE, Washington D.C., 2001), pp. 37.3.1–4.
[4] T. Low, M. F. Li, Y. C. Yeo, W. J. Fan, S. T. Ng, and D. L. Kwong, J. Appl. Phys. **98**, 024504 (2005).
[5] N. Neophytou, A. Pual, M. S. Lundstrom, and G. Klimeck, IEEE Trans. Electron devices **55**, 1286 (2008).
[6] L. Donetti, F. Gámiz, B. Biel, and C. Sampedro, J. Appl. Phys. **114**, 073706 (2013).
[7] W. Kohn and L. J. Sham, Phys. Rev. **140**, A1133 (1965).
[8] J. P. Perdew and Y. Wang, Phys. Rev. B **45**, 13244 (1992).
[9] S. Baroni, S. Gironcoli, A. D. Corso, and P. Giannozzi, Rev. Mod. Phys. **73**, 515 (2001).
[10] J. P. Perdew, K. Burke, and M. Ernzerhof, Phys. Rev. Lett. **77**, 3865 (1996).
[11] S. Y. Matsushita, K. Matsui, H. Kato, T. Yamada, and S. Suto, J. Chem. Phys. **140**, 104709 (2014).
[12] S. Y. Matsushita, C. Hu, E. Kawamoto, H. Kato, K. Watanabe, and S. Suto, J. Chem. Phys. **143**, 214702 (2015).
[13] H. M. Tütüncü, E. Karaca, and G. P. Srivastava, Surf. Sci. **647**, 17 (2016).
[14] A. A. Stekolnikov, J. Furthmüller, and F. Bechstedt, Phys. Rev. B **70**, 045305 (2004).
[15] N. D. Kim, Y. K. Kim, C.-Y. Park, H. W. Yeom, H. Koh, E. Rotenberg, and J. R. Ahn, Phys. Rev. B **75**, 125309 (2007).
[16] K. Sakamoto, M. Setvin, K. Mawatari, P. E. J. Eriksson, K. Miki, and R. I. G. Uhrberg, Phys. Rev. B **79**, 045304 (2009).
[17] S. Suto, K. Matsui, S. Y. Matsushita, H. Kato, H. Nakaya, T. Taoka, A. Kasuya, and T. Yamada, Appl. Surf. Sci. **267**, 90 (2013).
[18] S. Y. Matsushita, E. Kawamoto, K. Haga, T. Yamada, and S. Suto, Surf. Sci. **632**, 135 (2015).
[19] E. Kawamoto, J. Kang, T. Matsuda, T. Yamada, and S. Suto, Jpn. J. Appl. Phys. **56**, 025701 (2017).
[20] S. Souma, A. Takayama, K. Sugawara, T. Sato, and T. Takahashi, Rev. Sci. Instrum. **81**, 095101 (2010).
[21] S. Souma, T. Sato, T. Takahashi, and P. Baltzer, Rev. Sci. Instrum. **78**, 123104 (2007).
[22] P. Hohenberg and W. Kohn, Phys. Rev. **136**, B864 (1964).
[23] X. Gonze, F. Jollet, F. Abreu Araujo, D. Adams, B. Amadon, T. Applencourt, C. Audouze, J.-M. Beuken, J. Bieder, A. Bokhanchuk, E. Bousquet, F. Bruneval, D. Caliste, M. Côté, F. Dahm, F. Da Pieve, M. Delaveau, M. Di Gennaro, B. Dorado, C. Espejo, G. Geneste, L. Genovese, A. Gerossier, M. Giantomassi, Y. Gillet, D. R. Hamann, L. He, G. Jomard, J. Laflamme Janssen, S. Le Roux, A. Levitt, A. Lherbier, F. Liu, I. Lukačević, A. Martin, C. Martins, M. J. T. Oliveira, S. Poncé, Y. Pouillon, T. Rangel, G.-M. Rignanese, A. H. Romero, B. Rousseau, O. Rubel, A. A. Shukri, M. Stankovski, M. Torrent, M. J. Van Setten, B. Van Troeye, M. J. Verstraete, D. Waroquiers, J. Wiktor, B. Xu, A. Zhou, and J. W. Zwanziger, Comput. Phys. Commun. **205**, 106 (2016); The ABINIT code is a common project of the Université Catholique de Louvain, Corning Incorporated, and other contributors, http://www.abinit.org.
[24] N. Troullier and J. L. Martins, Phys. Rev. B **43**, 1993 (1991).
[25] S. Goedecker, M. Teter, and J. Hutter, Phys. Rev. B **54**, 1703 (1996).
[26] See Supplemental Material at http://link.aps.org/supplemental/10.1103/PhysRevB.96.125302 for (1) reading peak positions and shoulders in the energy distribution curves, (2) calculated energy bands of H:Si(110)-(1×1) and clean Si(110)-(1×1) surfaces, and (3) calculated energy bands of H:Si(110)-(1×1) surface for different slab thickness.
[27] I. Ivanov, A. Mazur, and J. Pollmann, Surf. Sci. **92**, 365 (1980).
[28] J. J. Yeh and I. Lindau, At. Data Nucl. Data Tables **32**, 1 (1985).
[29] J. Krempaský, H. Volfová, S. Muff, N. Pilet, G. Landolt, M. Radović, M. Shi, D. Kriegner, V. Holý, J. Braun, H. Ebert, F. Bisti, V. A. Rogalev, V. N. Strocov, G. Springholz, J. Minár, and J. H. Dil, Phys. Rev. B **94**, 205111 (2016).
[30] K. Hricovini, R. Günther, P. Thiry, A. Taleb-Ibrahimi, G. Indlekofer, J. E. Bonnet, P. Dumas, Y. Petroff, X. Blase, X. Zhu, S. G. Louie, Y. J. Chabal, and P. A. Thiry, Phys. Rev. Lett. **70**, 1992 (1993).
[31] S. Gallego, J. Avila, M. Martin, X. Blase, A. Taleb, P. Dumas, and M. C. Asensio, Phys. Rev. B **61**, 12628 (2000).
[32] Y. He, S. Bouzidi, B.-Y. Han, L.-M. Yu, P. A. Thiry, R. Caudano, and J.-M. Debever, Phys. Rev. B **54**, 17654 (1996).
[33] H. M. Fretwell, A. Kaminski, J. Mesot, J. C. Campuzano, M. R. Norman, M. Randeria, T. Sato, R. Gatt, T. Takahashi, and K. Kadowaki, Phys. Rev. Lett. **84**, 4449 (2000).
[34] T. Takahashi, G. Yamahata, J. Ogi, T. Kodera, S. Oda, and K. Uchida, in *Proceedings of the IEEE International Electron Devices Meeting Technical Digest* (IEEE, Baltimore, 2009), pp. 19.7.1-4.
[35] K. Uchida, A. Kinoshita, and M. Saitoh, in *Proceedings of the IEEE International Electron Devices Meeting Technical Digest* (IEEE, San Francisco, 2006).